

A two-step model for assessing the potential of shale-derived chemicals by oxidation of kukersite

Birgit Mets^(a), Margus Lopp^(a), Jaan Mihkel Uustalu^(a), Kati Muldma^(a), Allan Niidu^(b), Kristiina Kaldas^{(a)*}

^(a) Industrial Chemistry Laboratory, Department of Chemistry and Biotechnology, Tallinn University of Technology, Ehitajate tee 5, 19086 Tallinn, Estonia

^(b) Virumaa College, School of Engineering, Tallinn University of Technology, Järveküla tee 75, 30322 Kohtla-Järve, Estonia

Received 23 June 2023, accepted 13 October 2023, available online 10 November 2023

Abstract. The organic matter in oil shale (kerogen) contains vast potential as its structure is rich in easily convertible and versatile building blocks. Due to the complex structure of kerogen, simplifications are often used in order to obtain any information about the mechanism of its processing. This paper presents an approximate two-stage kinetic model which has been constructed to describe the wet air oxidation (WAO) process of the kerogen of Estonian kukersite oil shale, i.e. an alternative oil shale treatment process. The results obtained highlight the basic mechanisms of oil shale oxidation by molecular oxygen in water into different products. These outcomes add to the already existing knowledge on the structure of kerogen and validate it. The composed two-stage reaction formula outlines a fast reaction period which describes the dissolution of organic material, followed by a slower oxidation of dissolved substances. The attained high dissolution rate of kukersite kerogen illustrates the potential for recovering feedstock chemicals. The rate constants found remained independent of the oxygen-to-carbon ratio and good agreement was observed between calculated kinetic curves and experimental values.

Keywords: Estonian oil shale kukersite, organic matter, kerogen structure, oxidation.

* Corresponding author: e-mail kristiina.kaldas@taltech.ee

© 2023 Authors. This is an Open Access article distributed under the terms and conditions of the Creative Commons Attribution 4.0 International License CC BY 4.0 (<http://creativecommons.org/licenses/by/4.0>).

1. Introduction

Estonian oil shale, named kukersite, is a sedimentary rock from the Ordovician era containing up to 50% of organic matter (kerogen) [1–3]. To produce oil and chemicals, the cross-linked macromolecular structure of kerogen must be partially decomposed to low molecular weight organic compounds. The most common conversion process for oil shale is pyrolysis at temperatures over 400 °C, producing shale oil and some fine chemicals as by-products (phenolic compounds). The oil products from Estonian kukersite oil shale are a complex mixture of hydrocarbons and aromatic compounds, and, unlike oil from conventional crude, have a high oxygen content [4–6]. Alkyl resorcinols are the most characteristic group of oxygen-containing compounds in shale oil.

Another possibility for disintegrating oil shale macromolecular matrix is partial oxidation. In order to investigate the air oxidation process of kerogen and the associated CO₂ formation, the information about kerogen structure is essential. The proposal about the origination of oil shale mainly from *Gloeocapsomorpha prisca* microorganisms was made by Fokin [7] as early as a hundred years ago. Later, Blokker et al. [8] showed by means of RuO₄ oxidation that the kerogen matrix of kukersite mainly consists of resorcinol units linked by hydrocarbon chains. This suggestion is well consistent with the findings of Lille [9] and Burdelnaya [10], who analysed the structural fragments in kukersite by the means of ¹³C NMR. The reported estimates of aromatic carbon content in kukersite are in the range of 15–22% [9–12].

In order to develop technologies which would directly produce valuable dicarboxylic acids from oil shale, both nitric acid [13–16] and molecular oxygen in a non-catalytic process [17, 18] have been used. In the previous studies by Kaldas et al. [19, 20], the results of wet air oxidation (WAO) applied to oil shale concentrates at temperatures up to 200 °C were presented. The aim was to explore the potential for obtaining various feedstock chemicals through this advanced oxidation process. In wet air oxidation, oxygen reacts with the hydrocarbon-containing part of kerogen, resulting in decomposition primarily to carboxylic acids and other water-soluble substances. CO₂ gas is also formed concurrently with these reactions. Unlike the pyrolysis process, the conversion of kerogen with air can be achieved at significantly lower temperatures. An efficient dissolution of kerogen occurs even at 175 °C and 8 bar of oxygen, without the need for an external catalyst.

To the best of our knowledge, no previous attempt has been made to model the wet air oxidation of oil shale through kinetic calculations. Earlier, the focus has been on the mechanisms of shale oil formation, which are usually roughly divided into two sequential stages – first the formation of thermobitumen, then volatiles [21, 22]. This paper proposes that the oxidation of kukersite by molecular oxygen at significantly lower temperatures can also be formally divided into two distinctive steps and that these steps can be distinguished by CO₂ formation. The idea is based on the knowledge that

the organic structure of kukersite kerogen contains compounds with widely varying oxidation potentials. The authors of this paper have shown repeatedly that methylresorcinols are far more sensitive towards air oxidation than the rest of the kerogen or formed dicarboxylic acids due to the increased electron density on the aromatic ring [20, 23]. If oxidized as single compounds, methylresorcinols are decomposed into CO₂ within 1 hour at 175 °C with pO₂ 20 bar, together with the formation of acetic acid, formic acid and butanoic acid [24]. Detailed analysis of the reaction products of 5-methylresorcinol oxidation shows that resorcinol moieties follow a reaction pathway similar to that of phenol via the sequential oxidative destruction of benzoquinones [23]. Carboxylic acids that no longer contain double bonds in their hydrocarbon backbone remain in solution as compounds less prone to oxidation.

Therefore, the first step formally represents the decomposition of resorcinol subunits and leads to the formation of water-soluble partially oxygenated intermediates. The second step represents the further oxidation of the primary oxidized material into CO₂. However, as air oxidation processes are led by free radical reactions where several pathways run in parallel, the two stages are in mutual competition. Therefore, a kinetic model is needed for estimating the contribution of these competing stages and to evaluate at which conditions the highest value of dissolved organics emerges. It should also be noted that resorcinols can act as co-oxidants if placed in the same solution with oil shale or carboxylic acids, i.e. they can promote the oxidative decomposition of other inherent substances and thereby increase the amount of CO₂ emitted [20, 23].

In this paper, the formal kinetics of the formation of water-soluble organics, CO₂, and the amount of unreacted carbon during the oxidation of kerogen by oxygen was investigated. The findings of the paper are a good example of whether and how the behaviour of a complex material, like kerogen, can be predicted based on a limited amount of data when considering the general elemental composition and structural model of kerogen. A kinetic model of kerogen oxidation would allow modelling the course of the reaction, thereby enabling the prediction of the distribution of products in a wide range of reaction conditions, namely, varying the oxygen and oil shale concentrations. The obtained results were used to discuss the oxidation mechanism and the initial structure of kerogen and its resorcinol content. However, it should be kept in mind that this model is only valid for kukersite oil shale kerogen as it assumes the presence of oxygen-rich alkylresorcinols in the structure.

2. Materials and methods

2.1. Oil shale oxidation

Calculations were made using experimental data from previous publications [19, 20]. In these experiments, oil shale with the organic content enriched to 70% was used (hereafter referred to as K-70). Briefly, the 500-mL stainless

steel pressure reactor (4575A, Parr Instrument Company, Moline, IL, USA) was half filled with a water-K-70 slurry with concentrations of 20, 30 and 40 g/L. The volume of water added (200 ml) was kept constant throughout the experiments. The reactor was pressurized up to 40 bar with oxygen-nitrogen mixtures with oxygen concentrations of 21%, 50% or 100%. The reaction temperature was set to 175 °C in all cases, however, the starting time of the reaction was defined as the time when the reactor reached 170 °C. The reaction taking place during the first 10 min of heating from 20 to 170 °C was assumed to be negligible, as proved by a previous work by Kaldas et al. [20]. Due to gas expansion, the pressure increased to ca 60 bar. To be able to calculate the kinetic parameters of the reaction, separate experiments with varying reaction times from 0.33 to 5 hours were run.

2.2. Measurements

As described earlier, all three phases – gas, liquid and solid – were collected and analysed at the end of the reaction [19, 20]. The parameters measured included the content of oxygen and carbon dioxide in the gas phase, carbon in unreacted kerogen and carbon in the dissolved material. The elemental composition of organic matter and the dissolved organics was used to establish the organic carbon ratio between different phases. All insoluble material was considered to be unreacted kerogen even if it was probably oxygenated to some extent. Details about the used measuring instruments and procedures can be found elsewhere [20] and the data on which the calculations are based is presented in Tables S1 and S2 (in Appendices).

2.3 Kinetic calculations

Kinetic calculations were done numerically using the Generalized Reduced Gradient (GRG) solution method by easily available Excel Solver software.

3. Results and discussion

3.1. Material balances of the kerogen oxidation reaction

The two-step oxidation of kukersite is illustrated in Figure 1. During kerogen oxidation under oxygen excess, two distinctly different slopes for the rate of CO₂ formation can be observed, and the point of intersection occurs around 1 hour. Initially, the formation of the dissolved fractions of kerogen (referred to as the first step) proceeds in parallel with CO₂ formation. Once the initial kerogen is depleted, the overoxidation of the dissolved matter (referred to as the second step) begins to dominate. As a result, the average molecular weight of the remaining compounds decreases and the majority of the soluble fraction is composed of formic, acetic and succinic acids (C(C1–C4)) after a 5-hour reaction. However, it is evident that the rate of CO₂ emission during the second

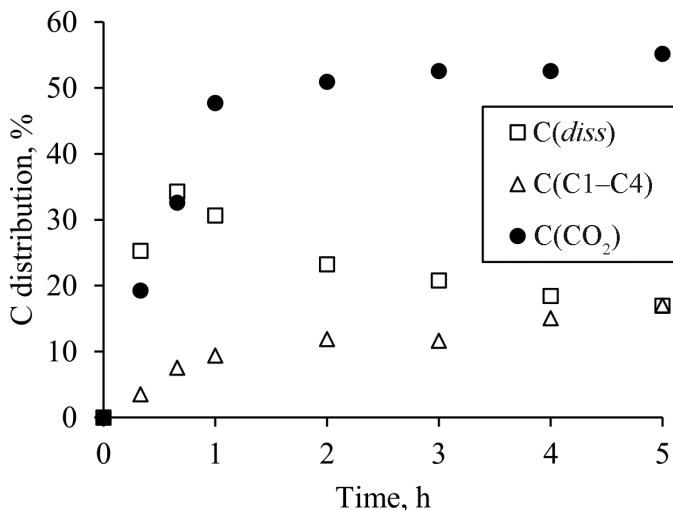


Fig. 1. Two-stage CO₂ release during kerogen air oxidation and associated organic carbon distribution in products. Reaction conditions: K-70 = 20 g/L, pO₂ = 40 bar; C(C1–C4) represents carbon in low molecular weight carboxylic acids.

stage is significantly lower than that of the initial oxidation of kerogen. During prolonged reaction times or at higher temperatures, the complete destruction of the organic kerogen skeleton occurs, resulting in the formation of CO₂ and water [19].

The oxidation of organic matter occurs in all three different aggregate states: solid kerogen, liquid (water, which partly dissolves the reaction products) and gaseous oxygen. The calculations are conducted based on the assumption that the reaction follows a two-stage process, wherein the initial stage involves the partial oxidation of solid kerogen, resulting in dissolved organic matter. The second stage involves the disintegration of the dissolved matter into carbon dioxide and water. Therefore, the oxidation reaction proceeds according to the following simplified sequence:



A theoretical solution for similar mixed-type reactions has been proposed [25]. However, a closed-form calculation for determining the differential equation cannot be employed in this case due to the need for optimization of various factors, including the amount of carbon dioxide in the first stage (represented by factor m), the amount of oxygen in the dissolved material (represented by factor n), as well as the rate constants k_1 and k_2 , for example, when the stoichiometry of the kerogen oxidation reaction is unknown. Therefore, the kinetic reaction rates were calculated numerically using the Generalized Reduced Gradient (GRG) solution method.

The elemental composition of K-70 is given in Table 1. From the values in Table 1 the carbon-based formal molecular formula of kerogen was calculated to be $\text{CH}_{1.39}\text{O}_{0.11}$.

Table 1. The chemical composition of the oil shale 70% concentrate sample, wt%

Parameter	C	H	N	S	O	TIC ^a	TOC ^{b*}	TOO ^{c*}
Value	57.8	6.7	0.16	0.7	19.1	1.3	56.5	8.5

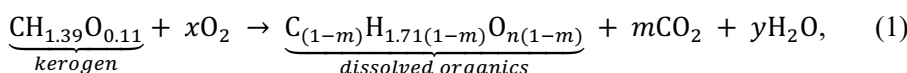
TIC^a – total inorganic carbon; TOC^b – total organic carbon; TOO^c – total organic oxygen; *calculated values.

When building the reaction model, the value of total organic oxygen must be used to exclude the oxygen in carbonate minerals as these do not participate in the oxidation reaction. The amount of organic and inorganic oxygen in kerogen was estimated by using the GOST 2408.3–95 standard method, which takes into account the content of ash, crystalline water and other components present in the material. Additionally, this work does not consider the oxidation of kerogen sulphur and nitrogen as their concentration in K-70 is low, and also due to the previous knowledge on WAO processes which suggests that most of the organic nitrogen and sulphur will be liberated as nitrates and sulphates [23].

For the dissolved organics, the measured oxygen content included partly soluble sulphates and other minerals (< 10 wt% of dissolved mass) as there is no standardized method for their separation without changing the composition of dissolved organics. An H/C balance of 1.71 with a standard deviation $\sigma = 0.2$ (see Table S2, Appendixes) was obtained from the results of the elemental analysis of the dissolved organics. The general formula for the dissolved organic subunit was calculated to be the following:



where n is a variable subject to this investigation and is assumed to be dependent on the $\text{O}_{2(aq)}/\text{C}_{ker}$ balance during the reaction ($\text{O}_{2(aq)}$ is the concentration of dissolved oxygen in the water phase and C_{ker} is the amount of carbon in kerogen). Based on the composition of kerogen, with the addition of x moles of oxygen, the oxidation reaction that converts one unit of kerogen into one unit of dissolved organic compound can be described by the following reaction (Eq. (1)):



where the parameter m is the amount of CO_2 generated from each carbon C_{ker} during the course of dissolution, reflecting the amount of formed CO_2 .

The total C balance for a subunit follows Equation (2):

$$C_{total} = I - m + m = I. \quad (2)$$

The total H balance for a subunit obeys Equation (3):

$$H_{total} = \underbrace{1.71(1 - m)}_{dissolved} + \underbrace{2y}_{H_2O} = \underbrace{1.39}_{initial\ kerogen}. \quad (3)$$

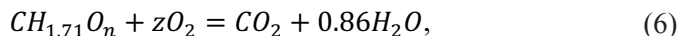
From Equation (3) y must have the following value (see Eq. (4)):

$$y = 0.86 - 0.15. \quad (4)$$

From Equations (1) and (3) the oxygen parameter x has the following value (see Eq. (5)):

$$x = n/2 (1 - m) - 0.13 + 1.39 m. \quad (5)$$

The second oxidation stage describes the oxidative decomposition of the dissolved organic material and is assumed to have the following formula (see Eq. (6)):



where

$$z = (2.85 - n)/2. \quad (7)$$

3.2. The kinetic equations

It is assumed that both these reactions (Eqns. (1) and (6)) proceed formally by the second-order reaction kinetics with rate constants k_1 and k_2 . Thus, the kinetic model for Equation (1) is as follows:

$$r_{C_{ker}} = -k_1[C_{ker}][O_{2(aq)}], \quad (8)$$

where $r_{C_{ker}}$ is the reaction rate for the disappearance of carbon in kerogen (with the unit mmol/(dm³s)). The corresponding rate equation for stage two is the following (Eq. (9)):

$$r_{C_{diss}} = -k_2[C_{diss}][O_{2(aq)}], \quad (9)$$

where $O_{2(aq)}$ is the concentration of oxygen in the liquid phase according to Henry's law ($O_{2(aq)} = H \cdot O_{2(g)}$), with Henry's constant $H = 8.94 \cdot 10^{-4}$ mol O₂/atm [26, 27]. Thus, reactions (8) and (9) (resp. Eqns. (8) and (9)) are both dependent on the partial pressure of oxygen.

From the balances in Equations (5) and (7) we get Equations (10) and (11):

$$\frac{dO_2 \text{ tot}}{dt} = \frac{dC_{ker}}{dt} \left(\frac{n}{2} (1 - m) - 0.13 + 1.39 m \right) + \frac{dC_{diss}}{dt} (2.85 - n)/2, \quad (10)$$

$$O_{2(tot)} = O_{2(aq)} + O_{2(g)}. \quad (11)$$

The rate of CO₂ development can be defined as Equation (12):

$$\frac{dCO_2}{dt} = m \frac{dC_{ker}}{dt} + \frac{dC_{diss}}{dt}. \quad (12)$$

The following data reflect the attempt to optimize the parameters n (the amount of oxygen in the dissolved organics) and m (the amount of CO₂ generated for each dissolved kerogen carbon unit) and the two rate constants k_1 and k_2 in such a way that the calculated reaction kinetics are as close to the experimental results as possible. These experimental results stem from 47 different measurement points, each comprising four distinct quantities. These quantities include O₂, carbon (C) in both kerogen (C_{ker}) and dissolved matter (C_{diss}), as well as CO₂. The experimental values were measured at 20, 40, 60, etc., minutes. The optimization was performed by minimizing the sum of squared difference between experimental and assumed kinetic functions. The numerical integration was performed at 20-second steps (dt).

The authors acknowledge that this model is a simplified representation of the real process, starting with the second-order reaction kinetics and considering the oxygen concentration in the liquid phase, which depends not only on the partial pressure of oxygen but also on the pressure of other gaseous ion concentrations in the water phase. However, the aim is to demonstrate the feasibility of such a minimalistic model to explore future possibilities for alternative uses of oil shale as a chemical feedstock.

3.3. The reaction model of oxidation

The calculated values from seven different combinations of oxygen concentrations and amounts of K-70 are presented in Table 2. The different experimental conditions are characterized by the amounts of oxygen dissolved and carbon in kerogen at the start of the reaction (O_{2(aq)}/C_{ker} at t = 0). The calculation considers the optimum values for seven different k_1 , k_2 , and n and one single m . Various test optimizations showed that the best fit for the system was when the value of parameter m was set constant for all the seven cases, e.g., further optimization was calculated with a mutual CO₂ development. This indicated that the kerogen decomposition yielded constant amounts of CO₂ independently of oxygen concentration. Table 2 shows the optimum value of m (-ΔCO₂/ΔC_{ker}) to be close to 0.2.

Table 2. The calculated reaction parameters for kerogen oxidation with oxygen

O ₂ conc., %	K-70, g	ΔO _{2(ag)} /ΔC _{ker} , mmol/mol	k ₁ , dm ³ /(mmol·s)	k ₂ , dm ³ /(mmol·s)	n, O in C _{diss}	m, ΔCO ₂ /ΔC _{ker}
100	4	56.1	1.65E-05	1.26E-06	1.73	
50	4	28.0	1.58E-05	2.14E-06	1.30	
50	6	18.8	1.48E-05	2.88E-06	0.85	
50	8	14.0	1.41E-05	1.51E-06	0.95	0.216
21	4	11.8	1.38E-05	6.82E-06	0.30	
21	6	7.8	1.31E-05	1.04E-05	1.22	
21	8	5.9	3.68E-05	2.93E-06	1.29	

conc. – concentration

Based on these data, kinetic curves were formed to compare the calculated and experimental values (Fig. 2).

Despite all the simplifications, the introduced two-stage oxidation model describes the experimental results reasonably well as indicated by a close fit between the experimental and calculated concentrations of C_{ker}, CO₂, C_{diss} and O₂ (see Fig. 2, (a)–(f)). The R² values were averaged for all measurands – oxygen in the gas phase and carbon in kerogen showed excellent fits (values of 0.95 and 0.99, respectively) and carbon as CO₂ exhibited an acceptable fit (0.9). For the dissolved carbon, the average R² was only 0.76, but this can be attributed to the complexity of analytical procedures – during evaporation, some volatile compounds were released. Therefore, the R² result for this parameter does not accurately describe the fit between the experimental and calculated results.

The values of k₁ and k₂ against O_{2(ag)}/C_{ker} are presented in Figure 3a. The variation of parameter n, which is the amount of oxygen in the dissolved organic matter, against the O₂/C_{ker} balance is presented in Figure 3b.

As can be seen from Figure 3a, the rate constants k₁ and k₂ were shown to be independent of the oxygen-to-carbon ratio at values higher than 15 mmol/mol, proving the validity of the model. The rate of dissolution is about one magnitude higher than the rate of complete oxidation to CO₂ and H₂O (as indicated by k₁>>k₂). This difference in reaction rates opens a window of opportunity to produce functional chemicals from the solid organic material called kerogen. The low conformity of the model with the experimental data at lower O₂ concentrations may be caused by the reduced solubility of O₂ which does not exactly follow Henry's law at low partial pressures. As is well discussed by other researchers, the overall kinetic regime of the wet air oxidation systems is not only dependent on the relative rates of the reactions occurring in the liquid

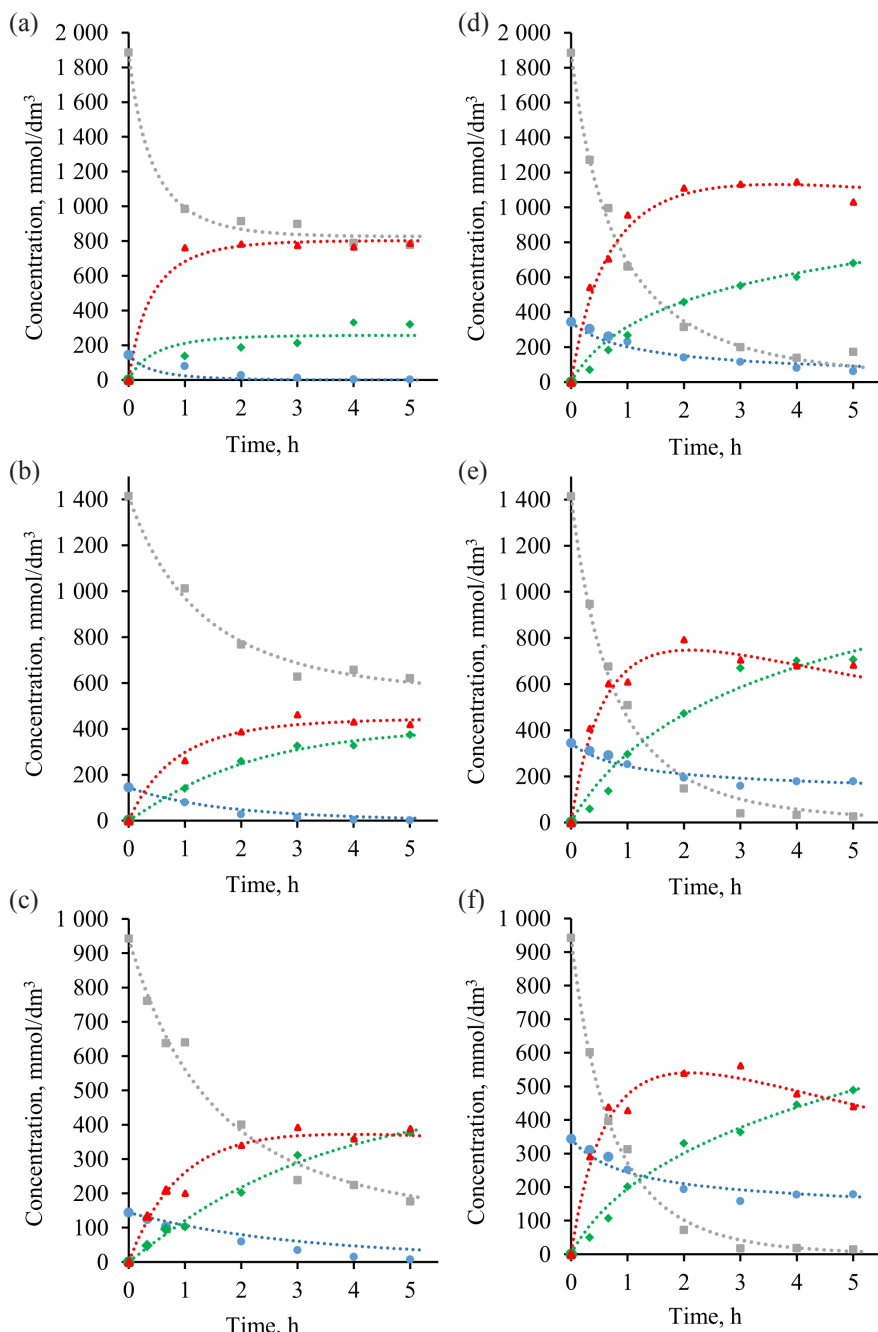


Fig. 2. Calculated (dashed lines) and experimental data (markers) for kerogen dissolution: (a) 21% O₂ and 8 g of K-70; (b) 21% O₂ and 6 g of K-70; (c) 21% O₂ and 4 g of K-70; (d) 50% O₂ and 8 g of K-70; (e) 50% O₂ and 6 g of K-70; (f) 50% O₂ and 4 g of K-70. The concentration of dissolved organic matter is marked in red colour, the increasing concentration of CO₂ in green, the decreasing concentration of kerogen in grey and the decreasing concentration of oxygen in blue. All units are mmol/dm³ of water volume, except oxygen, which is the amount of oxygen in mmol.

phase, but also on the mass transfer of oxygen from the gas phase to the liquid phase [28–30]. Both the decreased oxygen solubility and the ratio of oxygen gas to fluid at reduced partial pressures affect the oxygen transportation across the gas-liquid interface. Therefore, the overall oxidation process and the formation of oxidation promoting radicals proceed more slowly at lower oxygen concentrations. This indicates that the dissolution mechanism is following a different path at severe oxygen deficit, but this aspect is outside the scope of the present investigation.

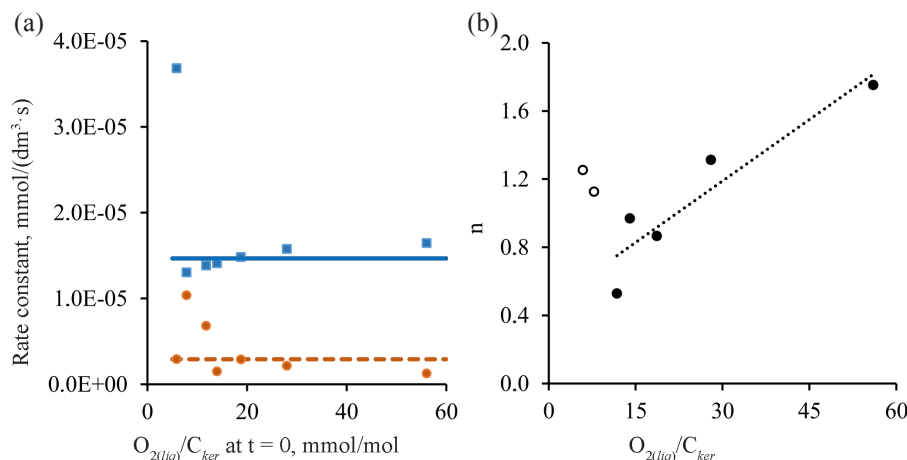


Fig. 3. (a) rate constants at different O_2/C_{ker} relations (blue – k_1 , orange – k_2); (b) variation of parameter n with O_2/C_{ker} balance (the trendline does not include 21% oxygen concentration kerogen loadings of 6 and 8 g).

Figure 3b reveals the oxygen content in the dissolved organics and shows that the amount of oxygen incorporated into the dissolved chemicals increased with higher oxygen concentrations. The values obtained for the O/C molar ratio of the dissolved material were in good accordance with the mean O/C values measured during experiments (0.8–1.3, Table S2), indicating the formation of highly oxygenated compounds such as low molecular weight dicarboxylic acids. The only exceptions are very low oxygen concentrations, showing once again that processes with insufficient oxygen have a different dissolution mechanism.

The reliability of the constructed model was tested through additional experiments under two different conditions, as indicated in Table 3.

Table 3. Experiments to test the reliability of the proposed model

Experiment	pO ₂ , bar	Time, h	C _{ker-initial} , mmol/dm ³	O ₂ , mmol	C _{ker} , mmol/dm ³	C _{CO₂} , mmol/dm ³	C _{diss} , mmol/dm ³
Fig. 4a	30	0.5	685.9	482.4	307.9	113.1	244.8
Fig. 4b	15	0.33	685.9	252.2	559.8	45.5	100.86

Using the average values of k_1 and k_2 , the corresponding computational curves for kerogen dissolution were generated based on the input oxygen and kerogen quantities. The relative difference between the experimental data (Fig. 4) and the corresponding calculated values for kerogen conversion and CO_2 formation is smaller than 15%, indicating a high level of precision in the model's assessment.

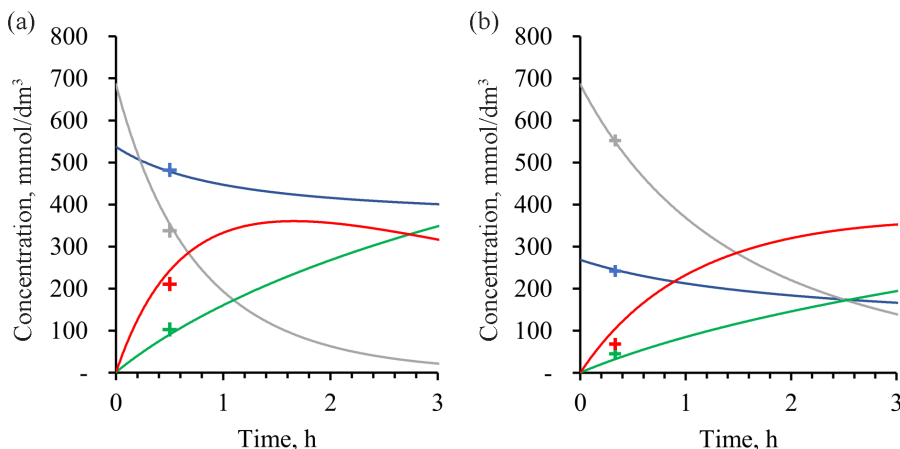


Fig. 4. Comparison of the proposed computational results (lines) with additional experimental data (crosses): (a) $K-70 = 20 \text{ g/L}$, $p\text{O}_2 = 15 \text{ bar}$, $t = 30 \text{ min}$; (b) $K-70 = 20 \text{ g/L}$, $p\text{O}_2 = 30 \text{ bar}$, $t = 20 \text{ min}$.

According to the proposed model, the CO_2 in the first stage of the process originates from the decomposition of resorcinol ring carbon. This suggestion is supported by the fact that the factor m was found to be 0.216, implying that ~22% of the oxidizing carbons are resorcinol-bound. This is in good agreement with the findings of other researchers showing that the resorcinol carbon content in kerogen is close to 21% [9, 10, 12]. Therefore, it can be proposed that the Lille-Blokker structural model of kukersite used by Mets et al. [31] may serve as a basis for identifying structure-based transformations for the further valorization of this fossil fuel, which could become a significant source of chemicals.

4. Conclusions

The results of this study have established that the oxidation process of oil shale kerogen with oxygen can be described kinetically as a two-step process. The presented approach provides a simple model for the oxidation of kukersite, highlighting the significant role of resorcinol units, particularly at the beginning of the oxidation process. Comparisons between the calculated kinetic curves

and experimental values demonstrated good agreement. Furthermore, it was observed that the rate constants remained independent of the oxygen-to-carbon ratio. The model showed limited conformity with experimental data at lower O₂ concentrations due to the reduced solubility of O₂. The dissolution rate was found to be approximately one order of magnitude higher than the rate of complete oxidation to CO₂ and H₂O, indicating the possibility of recovering dissolved compounds. Based on the determined value of *m*, which represents the amount of carbon released as CO₂ per carbon of oxidizing kerogen, it was concluded that kukersite likely contains around 22% resorcinols.

This data provides valuable insights into the alternative transformation process of kukersite kerogen and directs future experimental research in this area.

Acknowledgements

The authors are grateful to Kerogen Ltd. for financial support and Alexela Group Ltd. for technical support. We thank Oil Shale Competence Centre for fruitful cooperation and analysis of oil shale samples. We thank the Laboratory of the Department of Energy Technology in TalTech for carrying out compositional analysis. We are grateful to the entire Industrial Chemistry Laboratory team, both former and current members, including those who were not directly involved in the preparation of this article but showed their support in other ways. We also thank the editors and reviewers for valuable comments which improved the final manuscript.

The publication costs of this article were covered by the Estonian Academy of Sciences.

Appendices

Table 1S. Oxidation results

O ₂ , %	K-70, g	Time, h	O ₂ , mmol	C _{ker} , mmol/dm ³	C _{CO₂} , mmol/dm ³	C _{diss} , mmol/dm ³	C _{loss} , mmol/dm ³
100	4	0	703	943	—	—	—
100	4	0.33	641	387	182	239	135
100	4	0.66	573	89	308	324	222
100	4	1	542	33	450	289	170
100	4	2	512	27	481	219	216
100	4	3	493	22	496	196	228
100	4	4	508	21	496	174	251
50	4	0	343	943	0	0	0
50	4	0.33	310	602	50	67	224
50	4	0.66	291	397	107	169	270
50	4	1	252	313	201	283	145
50	4	2	194	72	330	249	291
50	4	3	158	17	363	194	368
50	4	4	177	18	446	158	320
50	4	5	178	14	488	132	308
50	6	0	343	1414	0	0	-
50	6	0.33	307	947	59	60	349
50	6	0.66	276	675	136	215	387
50	6	1	220	509	295	382	228
50	6	2	133	147	473	369	424
50	6	3	112	39	669	299	407
50	6	4	97	33	702	239	440
50	6	5	93	26	706	208	474
50	8	0	343	1885	0	0	0
50	8	0.33	304	1271	71	88	455
50	8	0.66	261	996	183	246	460
50	8	1	230	661	268	353	603
50	8	2	141	315	458	468	643

Table 1S. (continued)

O ₂ , %	K-70, g	Time, h	O ₂ , mmol	C _{ker} , mmol/dm ³	C _{CO₂} , mmol/dm ³	C _{diss} , mmol/dm ³	C _{loss} , mmol/dm ³
50	8	3	114	199	552	430	704
50	8	4	81	138	600	384	762
50	8	5	61	172	681	353	678
21	4	0	144	943	—	—	—
21	4	0.33	125	761	48	58	76
21	4	0.66	102	638	95	96	114
21	4	1	103	640	102	145	56
21	4	2	59	400	202	233	108
21	4	3	34	238	311	215	178
21	4	4	15	224	359	207	153
21	4	5	7	176	377	187	202
21	6	0	144	1414	—	—	—
21	6	1	79	1012	140	198	64
21	6	2	27	767	259	265	123
21	6	3	13	627	325	273	189
21	6	4	4	657	326	226	205
21	6	5	1	621	374	262	157
21	8	0	343	1885	0	0	0
21	8	0.33	304	1271	71	88	455
21	8	0.66	261	996	183	246	460
21	8	1	230	661	268	353	603
21	8	2	141	315	458	468	643
21	8	3	114	199	552	430	704
21	8	4	81	138	600	384	762
21	8	5	61	172	681	353	678

Note: C_{ker} is the concentration of carbon in the enriched oil shale K-70, C_{CO₂} is the amount of carbon bound in CO₂ (mmol), C_{diss} is the carbon bound to dissolved organics and C_{loss} is the carbon amount not accounted. In the calculations, C_{loss} is added to the dissolved carbon as it consists of lighter acids and other oxidized products formed from oil shale, such as formic and acetic acids. These smaller molecules have a lower boiling point and will evaporate during the drying of the dissolved material.

Table 2S. The elemental composition of dissolved material

O ₂ , %	C(K-70), g/L	Time, h	C(diss), g/L	N, %	C, %	H, %	S, %	TIC, %	O, %	H/C	O/C
100	20	0.33	6.8	0.18	41.84	4.95	2.31	n.d.	n.d.	1.4	n.d.
100	20	0.66	10.4	0.15	37.36	5.23	2.19	n.d.	n.d.	1.7	n.d.
100	20	1	9.6	0.18	36.33	5.09	2.79	n.d.	n.d.	1.7	n.d.
100	20	2	7.6	0.24	34.56	4.6	3.77	n.d.	n.d.	1.6	n.d.
100	20	3	7.4	0.24	31.62	4.99	3.76	n.d.	n.d.	1.9	n.d.
100	20	4	7.0	0.24	29.74	4.37	3.19	n.d.	n.d.	1.8	n.d.
100	20	5	6.5	0.47	28.33	4.27	3.66	n.d.	n.d.	1.8	n.d.
50	20	0.33	3.0	0.12	26.40	4.26	5.39	0.49	39.53	1.9	1.1
50	20	0.66	5.9	0.16	34.05	5.14	3.23	<LOD	42.53	1.8	0.9
50	20	1	9.4	0.21	36.09	5.71	2.62	<LOD	42.43	1.9	0.9
50	20	2	8.4	0.25	35.69	4.85	3.90	<LOD	n.d.	1.6	n.a.
50	20	3	7.4	0.32	31.52	4.85	4.14	<LOD	n.d.	1.8	n.a.
50	20	4	7.5	0.32	25.48	4.99	4.53	0.01	45.26	2.4	1.3
50	20	5	6.5	0.35	24.56	4.28	5.97	<LOD	n.d.	2.1	n.a.
50	30	0.33	3.8	0.11	23.55	3.71	5.99	0.94	39.00	1.9	1.2
50	30	0.66	8.1	0.15	31.88	5.18	3.21	<LOD	43.94	2.0	1.0
50	30	1	11.8	0.24	38.89	5.10	3.21	0.02	39.22	1.6	0.8
50	30	2	13.5	0.24	32.87	5.19	3.62	<LOD	36.26	1.9	0.8
50	30	3	10.7	0.37	33.51	5.57	2.08	<LOD	n.d.	2.0	n.a.
50	30	4	10.4	0.37	27.59	4.63	4.15	<LOD	45.20	2.0	1.2
50	30	5	9.0	0.39	27.67	4.19	4.96	0.10	n.d.	1.8	n.a.
50	40	0.33	4.3	0.11	24.41	3.86	5.60	0.85	42.11	1.9	1.3
50	40	0.66	8.5	0.17	34.79	4.65	3.24	0.01	40.42	1.6	0.9
50	40	1	11.3	0.17	37.42	4.72	2.58	<LOD	39.83	1.5	0.8
50	40	2	15.2	0.17	36.99	4.87	2.28	<LOD	39.47	1.6	0.8
50	40	3	15.0	0.17	34.34	5.15	2.29	<LOD	44.67	1.8	1.0
50	40	4	12.9	0.19	35.65	4.35	2.45	0.01	31.92	1.5	0.7
50	40	5	13.8	0.18	30.75	4.74	2.21	n.a.	40.11	1.9	1.0

Table 2S. (continued)

O ₂ , %	C(K-70), g/L	Time, h	C(diss), g/L	N, %	C, %	H, %	S, %	TIC, %	O, %	H/C	O/C
21	20	0.33	2.0	0.22	35.24	4.72	2.97	<LOD	n.d.	1.6	n.a.
21	20	0.66	3.6	0.17	31.54	5.00	2.75	<LOD	n.d.	1.9	n.a.
21	20	1	5.7	0.21	30.45	4.52	3.61	0.009	39.35	1.8	0.97
21	20	2	7.9	0.22	35.19	4.77	3.07	<LOD	38.69	1.6	0.82
21	20	3	7.4	0.24	34.84	4.83	3.80	<LOD	n.d.	1.7	n.a.
21	20	4	7.7	0.26	32.42	4.23	4.05	<LOD	42.10	1.6	0.97
21	20	5	6.7	0.29	33.65	4.25	3.25	<LOD	42.33	1.5	0.94
21	30	1	7.1	0.22	33.63	4.38	3.36	0.01	39.60	1.6	0.9
21	30	2	9.7	0.20	32.81	4.95	3.30	0.02	40.58	1.8	0.9
21	30	3	8.9	0.22	35.83	5.07	3.37	<LOD	n.d.	1.7	n.a.
21	30	4	8.8	0.18	30.71	4.77	3.94	<LOD	40.01	1.9	1.0
21	30	5	9.1	0.21	34.66	4.59	3.30	<LOD	39.73	1.6	0.9
21	40	1	6.3	0.13	27.47	3.78	4.04	1.09	32.31	1.7	0.9
21	40	2	9.4	0.17	32.99	4.41	3.54	0.03	33.72	1.6	0.8
21	40	3	11.1	0.09	25.73	4.95	2.93	<LOD	n.d.	2.3	n.a.
21	40	4	9.0	0.11	33.07	4.46	2.84	0.03	31.76	1.6	0.7
21	40	5	9.1	0.09	29.11	4.13	4.34	0.29	33.68	1.7	0.9

n.d. – not determined; n.a. – not applicable, as O, % is not determined; <LOD – below the limit of detection

REFERENCES

1. Francu, J., Harvie, B., Laenen, B., Siirde, A., Veiderma, M. *A Study on the EU Oil Shale Industry – Viewed in the Light of the Estonian Experience*. A report by EASAC to the Committee on Industry, Research and Energy of the European Parliament, 2007.
2. Dyni, J. R. Geology and resources of some world oil-shale deposits. *Oil Shale*, 2003, **20**(3), 193–252.
3. Speight, J. G. Oil shale resources. In: *Shale Oil Production Processes*. Gulf Professional Publishing, WY, USA, 2012, 35–73.
4. Baird, Z. S., Oja, V., Järvik, O. Distribution of hydroxyl groups in kukersite

- shale oil: Quantitative determination using Fourier transform infrared (FT-IR) spectroscopy. *Appl. Spectrosc.*, 2015, **69**(5), 555–562. <https://doi.org/10.1366/14-07705>
- 5. Järvik, O., Baird, Z. S., Rannaveski, R., Oja, V. Properties of kukersite shale oil. *Oil Shale*, 2021, **38**(4), 265–294. <https://doi.org/10.3176/oil.2021.4.01>
 - 6. Derenne, S., Largeau, C., Casadevall, E., Sinnighe Damsté, J. S., Tegelaar, E. W., de Leeuw, J. W. Characterization of Estonian Kukersite by spectroscopy and pyrolysis: Evidence for abundant alkyl phenolic moieties in an Ordovician, marine, type II/I kerogen. *Org. Geochem.*, 1990, **16**(4–6), 873–888. [https://doi.org/10.1016/0146-6380\(90\)90124-I](https://doi.org/10.1016/0146-6380(90)90124-I)
 - 7. Fokin, L. F. The structure and products of decomposition of Estonian bituminous rocks. *Gorny Zhurnal*, 1913, II, 117 (in Russian).
 - 8. Blokker, P., van Bergen, P., Pancost, R., Collinson, M. E., de Leeuw, J. W., Sinnighe Damsté, J. S. The chemical structure of *Gloeocapsomorpha prisca* microfossils: Implications for their origin. *Geochim. Cosmochim. Acta*, 2001, **65**(6), 885–900. [https://doi.org/10.1016/S0016-7037\(00\)00582-2](https://doi.org/10.1016/S0016-7037(00)00582-2)
 - 9. Lille, Ü., Heinmaa, I., Pehk, T. Molecular model of Estonian kukersite kerogen evaluated by ^{13}C MAS NMR spectra. *Fuel*, 2003, **82**(7), 799–804. [https://doi.org/10.1016/S0016-2361\(02\)00358-7](https://doi.org/10.1016/S0016-2361(02)00358-7)
 - 10. Burdelnaya, N. S., Bushnev, D. A., Mokeev, M. V. Changes in the composition of bitumen extracts and chemical structure of kerogen during hydrous pyrolysis. *Geochem. Int.*, 2013, **51**, 738–750. <https://doi.org/10.1134/S0016702913060037>
 - 11. Aarna, A. J., Lippmaa, E. T. On the structure of the Baltic oil shale kerogen. *Transact. Tallinn Polytechnic Institute*, Ser. A, 1955, **63**, 3–50 (in Russian).
 - 12. Chu, W., Cao, X., Schmidt-Rohr, K., Birdwell, J. E., Mao, J. Investigation into the effect of heteroatom content on kerogen structure using advanced ^{13}C solid-state nuclear magnetic resonance spectroscopy. *Energy Fuels*, 2019, **33**(2), 645–653. <https://doi.org/10.1021/acs.energyfuels.8b01909>
 - 13. Fomina, A., Pobul, L., Degterjowa, S., Veski, R., Kirret, O., Nikopensius, I., Männik, A., Pärn, A., Poom, A., Murumets, K., Ulanen, J., Tänav, I., Kotov, A. *Method for Processing Causticobiolites of the Sapropelite Type with an Oxidizing Agent*. German Patent No. 2259502, 1974.
 - 14. Degtereva, Z. A., Fomina, A. S. Production of dibasic acids $\text{C}_4\text{--C}_{10}$ from oil shale kukersite. *Acad. Sci. Est. SSR*, 1959, **8**(2), 122–136 (in Russian).
 - 15. Veski, R., Veski, S. Aliphatic dicarboxylic acids from oil shale organic matter – historic review. *Oil Shale*, 2019, **36**(1), 76–95. <https://doi.org/10.3176/oil.2019.1.06>
 - 16. Niudu, A., Grénman, H., Muldma, K., Kaldas, K., Mikli, V., Lopp, M. Behavior of Estonian oil shale in acidic oxidative conditions. *Front. Chem. Eng.*, 2022, **4**, 1–10. <https://doi.org/10.3389/fceng.2022.590115>
 - 17. Proskurjakov, V. A., Soloveichik, Z. V. Oxidation of oil shale by atmospheric oxygen. 2. Oxidation of Gdov shales with continuous air supply. *Trudy Vsesoj. N.I. Instituta po Pererabotke i Issl. Topliva*, 1961, **10**, 81–90 (in Russian).
 - 18. Proskurjakov, V. A., Yakovlev, V. I., Kudrjukov, O. I. Oxidation of oil shale

- by atmospheric oxygen. 3. Oxidation of common oil shales. *Trudy Vsesoj. N.I. Instituta po Pererabotke i Issl. Topliva*, 1962, **11**, 20–27 (in Russian).
- 19. Kaldas, K., Preegel, G., Muldma, K., Lopp, M. Wet air oxidation of oil shales: Kerogen dissolution and dicarboxylic acid formation. *ACS Omega*, 2020, **5**(35), 22021–22030. <https://doi.org/10.1021/acsomega.0c01466>
 - 20. Kaldas, K., Niidu, A., Preegel, G., Uustalu, J. M., Muldma, K., Lopp, M. Aspects of kerogen oxidative dissolution in subcritical water using oxygen from air. *Oil Shale*, 2021, **38**(3), 199–214. <https://doi.org/10.3176/oil.2021.3.02>
 - 21. He, L., Ma, Y., Yue, C., Li, S. Kinetic modeling of Kukersite oil shale pyrolysis with thermal bitumen as an intermediate. *Fuel*, 2020, **279**, 118371. <https://doi.org/10.1016/j.fuel.2020.118371>
 - 22. Astra, H. L., Albert, T., Mozaffari, S., Järvik, O., Yanchilin, A., Kamenev, S., Karagöz, S., Oja, V. Yields and the selected physicochemical properties of thermobitumen as an intermediate product of the pyrolysis of Kukersite oil shale. *Oil Shale*, 2021, **38**(4), 295–316. <https://doi.org/10.3176/oil.2021.4.02>
 - 23. Kaldas, K., Preegel, G., Muldma, K., Lopp, M. Reactivity of aliphatic dicarboxylic acids in wet air oxidation conditions. *Ind. Eng. Chem. Res.*, 2019 **58**(25), 10855–10863. <https://doi.org/10.1021/acs.iecr.9b01643>
 - 24. Kaldas, K. *Wet Air Oxidation of Oil Shale*. Ph.D. Thesis. Tallinn University of Technology, 2021.
 - 25. Lente, G. Analytical solutions for the rate equations of irreversible two-step consecutive processes with mixed second order later steps. *J. Math. Chem.*, 2017, **55**, 832–848. <https://doi.org/10.1007/s10910-016-0712-x>
 - 26. Pray, H. A., Schweickert, C. E., Minnich, B. H. Solubility of hydrogen, oxygen, nitrogen, and helium in water at elevated temperatures. *Ind. Eng. Chem.*, 1952, **44**(5), 1146–1151. <https://doi.org/10.1021/ie50509a058>
 - 27. Geng, M., Duan, Z. Prediction of oxygen solubility in pure water and brines up to high temperatures and pressures. *Geochim. Cosmochim. Acta*, 2010, **74**(19), 5631–5640. <https://doi.org/10.1016/j.gca.2010.06.034>
 - 28. Joglekar, H. S., Samant, S. D., Joshi, J. B. Kinetics of wet air oxidation of phenol and substituted phenols. *Water Res.*, 1991, **25**(2), 135–145. [https://doi.org/10.1016/0043-1354\(91\)90022-I](https://doi.org/10.1016/0043-1354(91)90022-I)
 - 29. Debellefontaine, H., Crispel, S., Reilhac, P., Périé, F., Foussard, J.-N. Wet air oxidation (WAO) for the treatment of industrial wastewater and domestic sludge. Design of bubble column reactors. *Chem. Eng. Sci.*, 1999, **54**(21), 4953–4959. [https://doi.org/10.1016/S0009-2509\(99\)00217-1](https://doi.org/10.1016/S0009-2509(99)00217-1)
 - 30. Kolaczkowski, S. T., Plucinski, P., Beltran, F.J., Rivas, F. J., McLurgh, D. B. Wet air oxidation: a review of process technologies and aspects in reactor design. *Chem. Eng. J.*, 1999, **73**(2), 143–160. [https://doi.org/10.1016/S1385-8947\(99\)00022-4](https://doi.org/10.1016/S1385-8947(99)00022-4)
 - 31. Mets, B., Kaldas, K., Uustalu, J. M., Lopp, M. The Lille-Blokker model – an excellent tool to describe the structure of kukersite. *Oil Shale*, 2023, **40**(3), 234–243. <https://doi.org/10.3176/oil.2023.3.04>